

Experimental Demonstration of Exceptional Points of Degeneracy in Linear Time-Periodic Systems and Exceptional Sensitivity

Hamidreza Kazemi¹, Mohamed Y. Nada¹, Alireza Nikzamir¹, Franco Maddaleno², Filippo Capolino¹

¹ Department of Electrical Engineering and Computer Science,
University of California, Irvine, CA 92697, USA and

² Department of Electronics and Telecommunications, Politecnico di Torino, 10129 Torino, Italy

We present the experimental demonstration of the occurrence of exceptional points of degeneracy (EPDs) in a single resonator by introducing a linear time-periodic variation of one of its components, in contrast to EPDs in parity time (PT)-symmetric systems that require two coupled resonators with precise values of gain and loss. In the proposed scheme, only the tuning of the modulation frequency is required that is easily achieved in electronic systems. The EPD is a point in a system parameters' space at which two or more eigenstates coalesce, and this leads to unique properties not occurring at other non-degenerate operating points. We show theoretically and experimentally the existence of a second order EPD in a time-varying single resonator. Furthermore, we measure the sensitivity of the proposed system to a small structural perturbation and show that the operation of the system at an EPD dramatically boosts its sensitivity performance to very small perturbations. Also, we show experimentally how this unique sensitivity induced by an EPD can be used to devise new exceptionally-sensitive sensors based on a single resonator by simply applying time modulation.

I. INTRODUCTION

Sensing and data acquisition is an essential part of many medical, industrial, and automotive applications that require sensing of local physical, biological or chemical quantities. For instance, pressure sensors [1, 2], temperature sensors [3], humidity sensors [4], and bio-sensors on the skin or inside the body have gained a lot of interest in the recent years [5–11]. Thus, various low-profile low-cost highly-sensitive electromagnetic (EM) sensing systems are desirable to achieve continuous and precise measurement for the mentioned various applications. The operating nature of the currently used EM resonant sensing systems are mostly based on the change in the equivalent resistance or capacitance of the EM sensor by a small quantity δ (e.g. 1%), resulting in changes of measurable quantities such as the resonance frequency or the quality factor that vary proportionally to δ (that is still in the order of 1%). The scope of this paper is to show theoretically and experimentally, a new strategy for sensing that leads to a major sensitivity enhancement based on a physics concept rather than just an optimization method, which forms a new paradigm in sensing technology.

In order to enhance the sensitivity of an EM system we exploit the concept of exceptional point of degeneracy (EPD) at which the observables are no longer linearly proportional to a system perturbation but rather have an m^{th} root dependence with m being the order of the EPD. Such dependence enhances the sensitivity greatly for small perturbations. For instance, exploiting an EPD of order 2 as in this paper, if we change a system capacitance by a small quantity δ (e.g., 1%) then the resonance frequency of a resonator operating at an EPD would change by a quantity proportional to $\sqrt{\delta}$ (e.g., 10%), making this fundamental physical aspect very interesting for sensing very small amounts of substances.

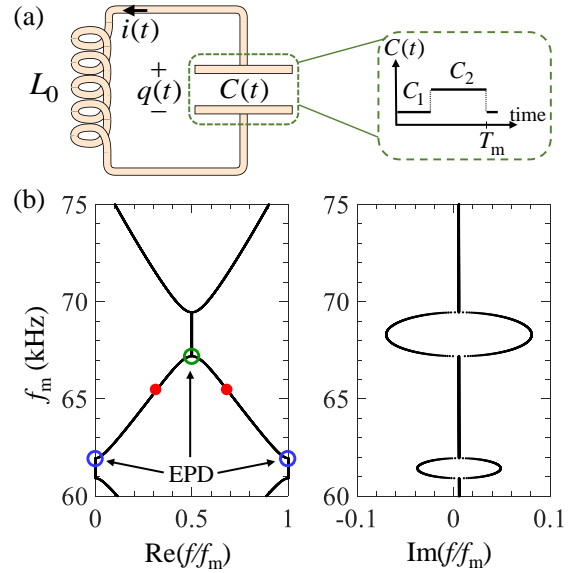


Figure 1. (a) Linear time-periodic LC resonator with a time-varying capacitor. The time-varying capacitance is a periodic piece-wise constant function as shown in the subset. (b) Dispersion diagram showing the real and imaginary parts of the eigenfrequencies of the resonator (i.e., the circuit's resonance frequencies) versus modulation frequency f_m of the capacitance. Due to time-periodicity, an EPD resonance at frequency f_{e0} has Fourier harmonics $f_{e0} + sf_m$, with $s = 0, \pm 1, \pm 2, \dots$

An EPD of order two is the splitting point (or degenerate point) of two resonance frequencies and it emerges in systems when two or more eigenmodes coalesce into a single degenerate eigenmode, in both their *eigenvalues* and *eigenvectors*. The emergence of EPDs is associated with unique properties that promote several potential applications such as enhancing the gain of active systems [12], lowering the oscillation threshold [13] or improving the

performance of laser systems [14, 15] or circuit oscillators [16], enhancing circuits' sensitivity at radio frequencies [2, 17–20] or at optical frequencies [21–24], etc.

EPDs emerge in EM systems using various methods: by introducing gain and loss in the system based on the concept of parity-time (PT-) symmetry [2, 15, 17–27], or by introducing periodicity (spatial or temporal periodicity) in waveguides [28–31]. Electronic circuits with EPD based on PT symmetry have been demonstrated in [17, 26] where the circuit is made of two coupled resonators with loss-gain symmetry, and only one precise combination of parameters leads to an EPD. The concept has been further elaborated in [2, 19] focusing on the high sensitivity of the EPD circuits introduced in [17, 26] to perturbations. Note that EPDs realized in PT-symmetric systems require at least two coupled resonators, and the precise knowledge and symmetry of gain and loss in the system. In contrast, in this paper we experimentally demonstrate EPDs that are directly induced via time modulation of a component in a *single* resonator [32]. An EPD induced by time modulation in a single resonator is easily tuned by just changing the modulation frequency of a component: this is a simple and viable strategy to obtain EPDs since the accurate change of a modulation frequency is common practice in electronic systems. Moreover, considering the fact that tuning of the modulation frequency is the key parameter to get an EPD, this strategy is also immune to tolerances in the values of commercially available inductors and capacitors.

In this paper we focus on the new scheme to obtain a second order EPD induced in a linear time periodic (LTP) system as introduced in [32]. Here EPDs are obtained by applying the time-periodic modulation to a system parameter (i.e., the capacitor) in a *single* resonator, and we provide an experimental demonstration of the existence of the LTP-induced EPD. Moreover, we show theoretically and experimentally how the resonance frequencies of a single EPD resonator are strongly perturbed by a tiny perturbation of its capacitor, and explore possible sensing applications of such phenomenon. We show that the system's resonance frequency shift generated by a perturbed EPD follows the Puiseux fractional power expansion series [33], i.e., if δ is a perturbation to a second order EPD system, two resonances arise shifted by a quantity proportional to $\sqrt{\delta}$ from the EP degenerate resonance frequency. On the other hand, perturbed systems not operating at an EPD exhibit a frequency shift proportional to δ , that is much smaller than $\sqrt{\delta}$ when $|\delta| \ll 1$. The theoretical predictions are in excellent agreement with the experimental demonstration, showing that tiny system perturbations can be detected by easily measurable resonance frequency shifts, even in the presence of electronic and thermal noise.

II. FORMULATION OF AN LTP-INDUCED EPD IN A SINGLE RESONATOR

We investigate resonances and their degeneracy in a linear time-periodic (LTP) LC resonator as shown in Fig. 1(a) where the time-varying capacitance is shown in the figure subset. This single-resonator circuit is supporting an EPD induced by the time-periodic variation. We consider a piece-wise constant time-varying capacitance $C(t)$ with period T_m ; we have chosen the piece-wise function to make the theoretical analysis easier, yet the presented analysis is valid for any periodic function. A thorough theoretical study of this type of temporally induced EPDs has been presented in [32], here we focus on the energy transfer formulation of these EPDs, and we show the first practical implementation of the EPDs induced in LTP systems.

The state vector $\Psi(t)$ describing the system in Fig. 1 is two-dimensional (see Ref. [32] for N -dimensional), i.e., $\Psi(t) = [q(t), i(t)]^T$, where T denotes the transpose operator, $q(t)$ and $i(t)$ are the capacitor charge and inductor current, respectively. The temporal evolution of the state vector obeys the 2-dimensional first-order differential equation

$$\frac{d\Psi(t)}{dt} = \underline{\mathbf{M}}(t)\Psi(t), \quad (1)$$

where $\underline{\mathbf{M}}(t)$ is the 2×2 system matrix. The 2-dimensional state vector $\Psi(t)$ is derived at any time $t = nT_m + \chi$ with n being an integer and $0 < \chi < T_m$ as

$$\Psi(t) = \underline{\Phi}(\chi, 0) [\underline{\Phi}(T_m, 0)]^n \Psi(0), \quad (2)$$

where $\underline{\Phi}(t_2, t_1)$ is the 2×2 state transition matrix [32] that translates the state vector from the time instant t_1 to t_2 . The state transition matrix is employed to represent the time evolution of the state vector, hence we formulate the eigenvalue problem as [32]

$$(\underline{\Phi} - \lambda \underline{\mathbf{I}})\Psi(t) = 0. \quad (3)$$

The two eigenvalues are $\lambda_p = \exp(j2\pi f_p T_m)$, $p = 1, 2$, where f_p are the system resonant frequencies, with all their Fourier harmonics $f_p + sf_m$, where s is an integer and $f_m = 1/T_m$ is the modulation frequency. Fig. 1(b) shows the dispersion diagram of the resonant frequencies varying modulation frequency f_m , restricting the plot to frequencies in the range $0 < f/f_m < 1$, which is called here as the fundamental Brillouin zone (BZ), adopting the language used in space-periodic structures. The two red circles in Fig. 1(b) corresponds to two general distinct resonant frequencies at f and $-f + f_m$ with positive real part. An EPD occurs when these two resonance frequencies coalesce at a given modulation frequency. At an EPD the transition matrix $\underline{\Phi}$ is non-diagonalizable with

a degenerate eigenvalue λ_e (with corresponding eigenfrequency ω_e) because the two eigenvalues and two eigenvectors coalesce. Two possibilities may occur because of the nature of the problem (time periodicity, because there are only two possible eigenmodes, and neglecting losses for a moment): the degenerate eigenvalue is either i) $\lambda_e = -1$, corresponding to an eigenfrequency of $f_{e0} = f_m/2$ and its Fourier harmonics $f_{es} = f_{e0} + sf_m$ shown with the green circles in Fig. 1(b), or ii) $\lambda_e = 1$, corresponding to $f_{e0} = 0$ and its Fourier harmonics $f_{es} = f_{e0} + sf_m$ shown with a blue circle in Fig. 1(b). Therefore, in general an EPD resonance is characterized by the fundamental frequency f_{e0} and all harmonics at $f_{es} = f_{e0} + sf_m$ where $s = 0, \pm 1, \pm 2, \dots$. Moreover, at an EPD the state transition matrix $\underline{\Phi}$ is similar to a Jordan-Block matrix of second order, hence it has a single eigenvector, i.e., the geometrical multiplicity of the eigenvalue λ_e is equal to 1 while its algebraic multiplicity is equal to 2. Considering the circuit parameters given in the next section including inductor small series resistance, an EPD occurs at $f_m = 62.7$ kHz, leading to a degenerate resonance frequency of $f_{e0}/f_m = j0.0041$ which corresponds to blue circle in Fig. 1(b). Another EPD occurs at $f_m = 67.7$ kHz, leading to a degenerate resonance frequency of $f_{e0}/f_m = 0.5 + j0.0038$ which corresponds to green circle in Fig. 1(b).

When $\lambda_e = -1$ and hence $f_{e0} = f_m/2$, i.e., for EPDs at the center of the BZ, the state transition matrix $\underline{\Phi}$ has a trace of -2 [32], so that we express $[\underline{\Phi}(T_m, 0)]^n$ as [34]

$$[\underline{\Phi}(T_m, 0)]^n = (-1)^{n+1} [n\underline{\Phi}(T_m, 0) + (n+1)\mathbf{I}], \quad (4)$$

where \mathbf{I} is the 2×2 identity matrix. Thus, we reformulate (2) using (4) as

$$\Psi(t) = (-1)^{n+1} [n\underline{\Phi}(T_m, 0) + (n+1)\mathbf{I}]\underline{\Phi}(\chi, 0)\Psi(0). \quad (5)$$

Similarly, for EPDs at the edge of the BZ, i.e., when $\lambda_e = 1$ and $f_{e0} = 0$, the transition matrix $\underline{\Phi}$ has a trace equal to 2, and [34]

$$[\underline{\Phi}(T_m, 0)]^n = n\underline{\Phi}(T_m, 0) - (n-1)\mathbf{I}, \quad (6)$$

hence

$$\Psi(t) = [n\underline{\Phi}(T_m, 0) - (n-1)\mathbf{I}]\underline{\Phi}(\chi, 0)\Psi(0). \quad (7)$$

Because of the multiplication of the time-period step n , we conclude from Eqs. (5) and (7) that when the system is at the second order time-periodic induced EPD, the state vector grows linearly with time. This linear growth is expected and it is one of the unique characteristics associated with EPDs. This algebraic growth is analogous to the spatial growth of the state vector associated with the space-periodic EPDs [12, 30].

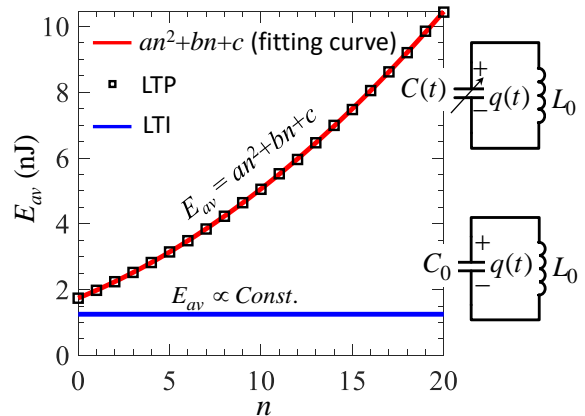


Figure 2. Comparison between the time-average energy stored in a lossless, linear time-invariant LC resonator (solid blue line) and the time-average energy stored in a linear time-periodic LC resonator operating at an EPD located at the edge of BZ (black square symbols) where n is an integer representing the number of elapsed modulation periods. In the latter case the time-average energy grows with time, fitted by a second order polynomial curve (red solid line). The fitting coefficients are set as $a = 0.01$, $b = 0.23$, and $c = 1.74$.

The time-periodic LC tank considered in this section is not “isolated”. In such a system, the time-varying capacitor is in continuous interaction with the source of the time variation that is exerting work. This interaction leads to a net energy transfer into or out of the LC tank; at some operating modulation frequencies the system simply loses energy to the time-variation source, while at other operating modulation frequencies the LC tank receives energy from the source of time variation. This behavior is in contrast to the behavior of a time-invariant lossless LC tank where the initial energy in the system is conserved and the net energy gain or loss is zero. The average transferred energy into or out of the time-periodic LC tank can be calculated using the time-domain solution of the two-dimensional first-order differential equation (7). Figure 2 shows the calculated time-average energy transferred into a linear time-invariant (LTI) lossless LC tank (solid blue line) and into an LTP one operating at a second order EPD (black square symbols), where $n = 0$ shows the average energy of the systems within the first period. The capacitor in both systems is initially charged with an initial voltage of $V_C(0^-) = -50$ mV. In the LTP system, the modulation frequency is adjusted to $f_m = 62.7$ kHz, so that it operates at the EPD denoted by the blue circles in Fig. 1(b). Note that the system is periodic, so that for an eigenfrequency f_p , there are also all the Fourier harmonics with frequencies $f_p + sf_m$, where s is an integer [32]. It is clear that the total energy in a lossless time-invariant LC resonator is constant over time while the average energy in the time-periodic LC resonator is growing at the EPD. This energy growth is quadratic in time since the state vector (i.e., capacitor charge and inductor current) of a periodically time-variant LC res-

onator experiencing an EPD grows linearly with time, as shown in Eqs. (5) and (7). Indeed, the solid red curve in Fig. 2 shows a second order polynomial curve fitted to the LTP LC resonator energy where the fitting coefficients are given in the figure caption. One may note from the figure that the average energy of the LTI and LTP systems are not equal at $n = 0$ which might seem counter intuitive. In fact, at $n = 0$ we show the average energy of the systems within the first time-period which is higher for the LTP system due to the energy transfer within that first period.

Note that the time-varying capacitance in our proposed scheme has some resemblance to the concept of parametric amplification [35–39]. However, in our single resonator proposed scheme, we use time-periodicity of a system parameter to achieve an EPD [32], and show high sensitivity of the degenerate resonance to system perturbations. In contrast, parametric amplifiers use time variation of a component as a non-conservative process to inject energy and generate amplification (which is not the case in our circuit), and generally possess low sensitivity to perturbations.

III. EXPERIMENTAL DEMONSTRATION OF AN EPD AND ITS SENSITIVITY TO PERTURBATIONS

In this section we verify *experimentally* the key properties inferred from the degeneracy of resonances shown in the dispersion diagram in Fig. 1 and we observe some interesting physical properties by providing an initial charge to the capacitor and measure the triggered time domain natural response. The time varying LC tank with the time-periodic capacitor is implemented based on the scheme shown in Fig. 3(a). The time variation is carried out using a time-varying *pump* voltage $v_p(t)$ and a multiplier. Hence the voltage applied to the capacitor C_0 is equal to $v_c(t) = v(t)[1 - v_p(t)/V_0]$, where $v(t)$ is the voltage of Node A with respect to the ground, and the term V_0 is a constant coefficient of the multiplier that is used to normalize its output voltage. Here we are interested in having an LC resonator with a time varying capacitor $C(t)$ seen by the current $i_c(t)$ exiting the inductor and by the voltage $v(t)$ at Node A, hence satisfying the two equations $q(t) = C(t)v(t)$ and $di_c/dt = -v(t)/L_0 = -q(t)/(L_0C(t))$. This leads to the definition of the time varying capacitance $C(t) \triangleq C_0(1 - v_p(t)/V_0)$ and to a LTP LC circuit described by Eq. (1) (see Supplement Material), which in turns leads to the time domain dynamics exhibiting EPDs as described in [32].

In such a LTP LC circuit, the time variation behavior of the capacitance is dictated by the variation of the pump voltage $v_p(t)$, therefore to design the time-varying capacitance shown in Fig. 1(a) we apply a two level piece-wise constant pump voltage to the multiplier. The values of C_1 and C_2 are adjusted by properly choosing the voltages of the piece-wise constant pump $v_p(t)$ as discussed

in the Supplement Material. We aim at designing the time-varying capacitor $C(t)$ with the values of $C_1 = 5$ nF and $C_2 = 15$ nF. Hence, the parameters of the circuit are set as $C_0 = 10$ nF, the two levels of the piece-wise constant time varying pump voltage as $v_p/V_0 = \pm 0.5$, and the period of the pump voltage as $T_m = 20$ μ s with 50% duty cycle. We verify the operation of this scheme using the finite difference time domain (FDTD) simulation implemented in Keysight ADS, where a constant capacitor C_0 is connected to the voltage multiplier. The time-varying capacitance, calculated as the ratio of the current passing through the capacitor C_0 to the time-derivative of the voltage at Node A, i.e., $i_c(t)/[dv/dt]$, is shown in Fig. 3(b). It is worth mentioning that in such a scheme, the *high* level of the pump voltage v_p controls the value of the capacitance C_1 and the *low* level controls the value of the capacitance C_2 .

Figure 3(c) illustrates the assembled circuit where the red dashed rectangle shows the implemented synthetic time-periodic capacitor $C(t)$. In this fabricated circuit we use a four-quadrant voltage output analog multiplier, a high stability and precision ceramic capacitor $C_0 = 10$ nF, and an inductor $L_0 = 33$ μ H with low DC resistance $R_{DC} = 108$ m Ω , as specified in the Supplement Material. As shown in Sec. II, we expect the capacitor voltage of the time-periodic LC tank to grow linearly in time when operating at an EPD; however, in practice it will saturate to the maximum output voltage of the multiplier. Therefore, to avoid voltage saturation, we have implemented a reset mechanism to reset the resonator circuit, where the reset signal is a digital clock with 20% duty cycle (i.e., $v_{reset} = 2$ V for 20% of its period and $v_{reset} = 0$ V otherwise) that allows the resonator circuit to run for the duration of the low voltage $v_{reset} = 0$ V. During the reset time, the reset signal is high $v_{reset} = 2$ V, and the resonator circuit is at pause. At the end of this time interval the capacitor is charged again with the initial voltage of $V_C(0^-) = -50$ mV for the start of the next working cycle as detailed in the Supplement Material. The circuit is provided with ± 5 V DC voltage using a Keysight E3631A DC voltage supply. We use two Keysight 33250A function generators, one to generate a two level piece-wise constant signal with levels of ± 0.525 V, duty cycle of 50% and variable modulation frequency f_m as pump voltage $v_p(t)$ to generate the time-periodic capacitance $C(t)$. The other function generator provides the resonator's reset signal, a two level piece-wise constant signal with levels of 2 V and 0 V, with duty cycle of 20% and frequency of 1.1 kHz (much lower than f_m).

A. Dispersion diagram and time domain response

Figure 4(a) presents the dispersion diagram as a function of the capacitance's modulation frequency f_m , which is experimentally varied by adjusting the frequency of the pump voltage $v_p(t)$. The solid curve denotes the theoretic

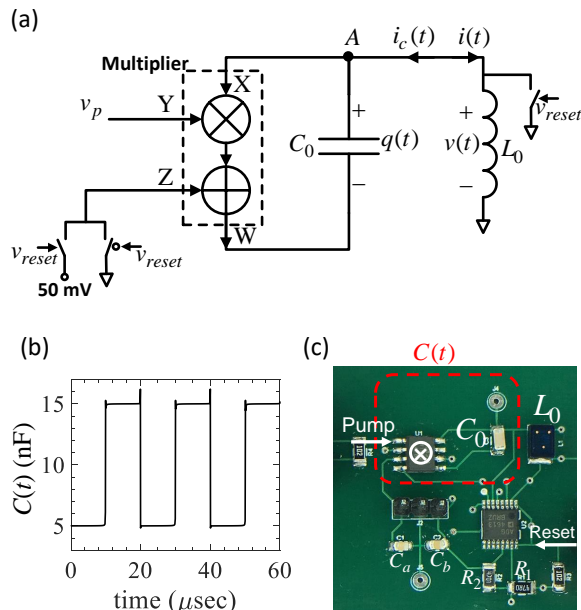


Figure 3. (a) Schematic of the LTP-varying LC resonator using the periodic pump voltage $v_p(t)$ and a multiplier. The reset switches are used in the implementation to avoid saturation and to add the initial voltage at the beginning of each “run” time. (b) Time domain simulations of the time-varying synthetic capacitance with period T_m seen from Node A with respect to the ground. (c) Assembled circuit where the red dashed square shows the synthetic time-varying capacitor using the pump voltage and a multiplier. The circuit also consists of the inductor L_0 , the reset circuit with switches, the regulating capacitors C_a and C_b , and the circuitry to produce the initial voltage (see Supplement Material).

cal dispersion diagram whereas red square symbols represent the experimental results. The experimental results are obtained by calculating the resonance frequency of the circuit’s response for different modulation frequencies using Fourier transform of the time domain signal triggered by the initial voltage $V_C(0^-)$ at each working cycle, where we used a Keysight DSO7104A digital oscilloscope to capture the time domain output signal. A good agreement is observed between the theoretical and experimental results, however, there is a slight frequency shift between the theoretical and experimental dispersion diagrams which is due to parasitic reactances, components’ tolerances and nonidealities in the fabricated circuit. Note that in Figure 4(a) we show only solutions in the first Brillouin zone defined here as $\text{Re}(f) \in (0, f_m)$. Since the system is time periodic, every mode is composed of an infinite number of harmonics with frequencies $f + sf_m$, where s is an integer. One can observe from the dispersion diagram that the time-periodic LC resonator operates at three different regimes depending on the modulation frequency. In the following we describe the three possible regimes of operation.

i) *Real resonances*: This is a regime where the system has two purely real oscillating frequencies (though

in practice there is a small imaginary part due to the finite quality factor of the components). Point #2 with the magenta circle in Fig. 4(a) illustrates a mode part of this regime, with real resonance frequencies f , and all its harmonics $f + sf_m$, where s is an integer. The signal has also the resonance frequency at $-f + f_m$, and hence also the harmonics at $-f + sf_m$. This means that two resonance modes with frequencies f and $-f + f_m$ are allowed. Fig. 4(c) shows the corresponding time domain signal at $f_m = 66.5$ kHz which corresponds to two almost-real resonance frequencies and their harmonics. As mentioned, the observed small exponential decay of the response is due to the finite quality factor of the components. In an ideal lossless system frequencies would be purely real.

ii) *Unstable condition*: This is a regime where the system has two complex resonance frequencies with imaginary parts of opposite signs (point #4 with the orange circle in Fig.4(a)). According to the time convention $e^{j\omega t}$, the state vector of the system corresponding to a complex resonance frequency with an imaginary part of negative sign shows an exponential growth, while the state vector corresponding to the resonance with an imaginary part with positive sign exhibits an exponential decay, hence it shows an unstable system. The exponentially growing behavior would be the dominant one and it is the one seen in the time domain response in Fig. 4(e) that would eventually saturate, if we did not include a reset circuit. In this case the modulation frequency of the pump voltage is set to $f_m = 71.5$ kHz. iii) *Exceptional points of degeneracy*: An EPD is the point that separates the two previous regimes, where two frequency branches of the dispersion diagram (describing two independent resonance solutions) coalesce. Indeed at the EPD the two resonant modes of the system coalesce and, as discussed in the previous section, the state vector shows a linear growth with time yet the resonance frequencies are real (when neglecting the small positive imaginary part of the resonance frequency due to finite quality factor of the components). From the theoretical analysis and from the experimental results in Fig. 4(a) one may note two types of EPDs exist in a linear time-periodic system [32]. EPDs that exist at the center of the BZ, i.e., at $f_{e0} = 0.5f_m$, with Fourier harmonics located at $f_{es} = (0.5 + s)f_m$, where the integer s denotes the harmonic number. An example of such a type of EPDs is observed at $f_m = 68.3$ kHz and is denoted by point #3 with the green circle in Fig. 4(a). The measured time domain behavior of the circuit at this modulation frequency is shown in Fig. 4(d) where we clearly see the linear growth of the capacitor voltage. It grows until it reaches saturation or till the system is reset as described in the previous section. The other type of EPDs are those that exist at the edge of the BZ, i.e., at $f_{e0} = 0$, with Fourier harmonics located at $f_{es} = sf_m$. An example of this type of EPDs is denoted by point #1 with the blue circle at $f_m = 62.8$ kHz in Fig. 4(a). The measured time domain behavior of the circuit at such an EPD is depicted in Fig. 4(b). Note that the oscillation of the

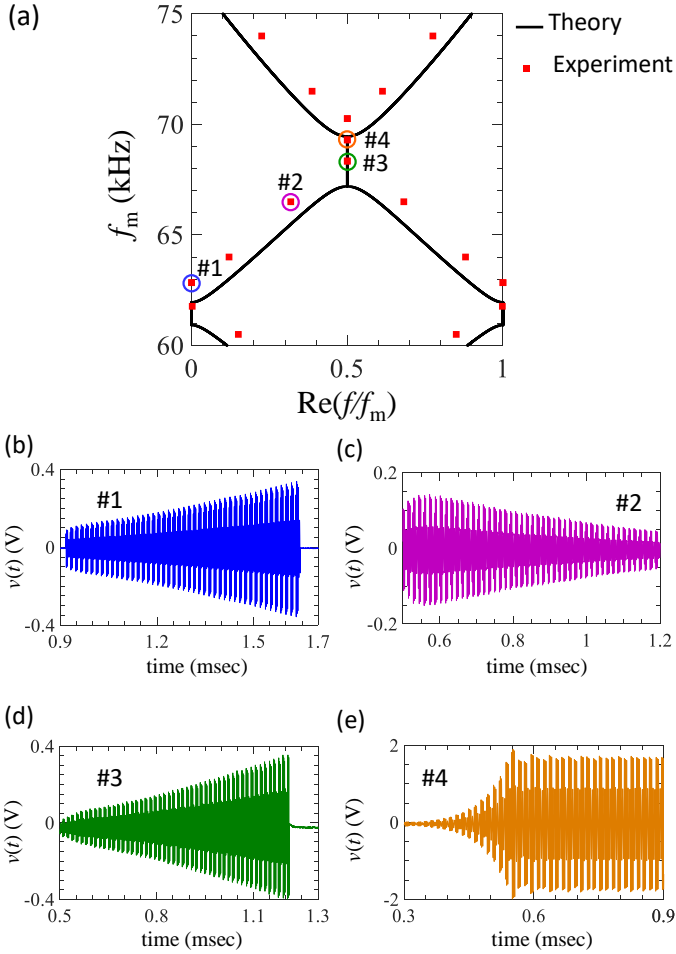


Figure 4. (a) Theoretical (solid lines) and experimental (square red symbols) results for the complex dispersion diagram showing the circuit's resonance frequencies as a function of modulation frequency f_m . (b-e) Time domain experimental results of the capacitor voltage at various modulation frequencies denoted by #1-4 in the dispersion diagram: (b) Exceptional point #1 denoted by the blue circle located at the edge of the BZ where the modulation frequency is $f_m = 62.8$ kHz. (c) Real-frequency resonance indicated by #2, denoted by the magenta circle, where the modulation frequency $f_m = 66.5$ kHz. (d) Exceptional point #3, denoted by the green circle, located at the center of the BZ where the modulation frequency is $f_m = 68.3$ kHz. (e) Unstable regime, point #4, denoted by an orange circle, represents two complex resonance frequencies, with opposite imaginary parts and real part equal to $f_m/2$, where the modulation frequency is set to $f_m = 71.5$ kHz. Note that due to time-periodicity, time domain signals have all Fourier harmonics $f + sf_m$, with $s = 0, \pm 1, \pm 2, \dots$

time domain signal for an EPD at the edge of the BZ is due to the harmonics located at sf_m .

One may observe that a standard “critically damped” LTI RLC circuit with two coinciding resonance frequencies is also an exceptional point, however, that point is characterized by two resonance frequencies with vanish-

ing real part; hence, it is a different condition from what we describe in this paper.

B. High sensitivity to perturbations

Sensitivity of a system's observable to a specific parameter is a measure of how strongly a perturbation to that parameter changes the observable quantity of that system. The sensitivity of a system operating at an EPD is boosted due to the degeneracy of the system eigenmodes. In the LTP system considered in this paper, a perturbation δ to a system parameter leads to a perturbed state transition matrix Φ and thus to perturbed eigenvalues $\lambda_p(\delta)$ with $p = 1, 2$. Therefore, the two degenerate resonance frequencies occurring at the EPD change significantly due to a small perturbation δ , resulting in two distinct resonance frequencies $f_p(\delta)$, with $p = 1, 2$, close to the EPD resonance frequency. The two perturbed eigenvalues near an EPD are represented using a convergent Puiseux series (also called fractional expansion series) where the Puiseux series coefficients are calculated using the explicit recursive formulas given in [33]. A first-order Puiseux approximation of $\lambda_p(\delta)$ is

$$\lambda_p(\delta) \approx \lambda_e + (-1)^p \alpha_1 \sqrt{\delta} \quad (8)$$

where α_1 is a coefficient that is either purely real or purely imaginary when losses can be neglected, and is given by

$$\alpha_1 = \sqrt{-\frac{\frac{dD(0, \lambda_e)}{d\delta}}{\frac{1}{2!} \frac{d^2 D(0, \lambda_e)}{d\lambda^2}}}. \quad (9)$$

where $D(\delta, \lambda) = [\det[\Phi(\delta) - \lambda \mathbf{I}]]$. Since this is a second order polynomial in λ , the denominator of (9) is equal to unity. The perturbed complex resonance frequencies are approximately calculated as

$$f_p(\delta) \approx f_{es} \pm j \frac{f_m}{2\pi} (-1)^p \alpha_1 \sqrt{\delta}, \quad (10)$$

where the \pm signs correspond to the cases with EPD either at the center ($f_{e0} = f_m/2$) or edge ($f_{e0} = 0$) of the BZ, respectively (we recall that in this paper the fundamental BZ is defined as $0 \leq f/f_m \leq 1$). Equation (10) is only valid for very small perturbations $\delta \ll 1$ and it is clear that for such a small perturbation the resonance frequencies f_p change dramatically from the degenerate resonance f_{es} due to the square root dependence $\Delta f = f_p(\delta) - f_{es} \propto \sqrt{\delta}$. Now, let us assume that the perturbation δ is applied to the value C_1 of the time-varying capacitor, and the perturbed C_1 is expressed as $(1+\delta)C_1$. Considering an unperturbed LTP LC resonator as shown in the subset of Fig. 1(a), the system has

a measured EPD resonance at a modulation frequency $f_m = 62.8$ kHz for the parameter values given in section III. This EPD resonance frequency is at $f_{e0} = 0$ Hz, corresponding to point #1 (blue circle) in the dispersion diagram shown in Fig. 4(a), and at all its Fourier harmonics $f_{es} = f_{e0} + sf_m$. By looking at the spectrum of the measured capacitor voltage we observe that among the various harmonics of such EPD resonance, the frequency of $\text{Re}(f_{e6}) = 6f_m = 374.2$ kHz has a dominant energy component, hence it is the one discussed in the following. The theoretical and experimental variations in the real part of the two perturbed resonance frequencies due to a perturbation $\delta \ll 1$ in the the time-variant LC circuit are shown in Fig. 5. Only the results for positive variations of δ are shown here, hence the resonances move in the directions where they are purely real (though the presence of small losses would provide a small imaginary part in the resonance frequency). The solid blue curve, dashed red curve, and green symbols denote the calculated-exact (solutions of Eq. (3) explained in Sec. II), Puiseux series approximation, and the experimentally observed resonance frequencies, respectively when varying δ . The coefficient α_1 in the Puiseux series is calculated to be $\alpha_1 = j2.65$ which according to the fractional expansion in Eq. (10) it implies only change of the real part of the resonance frequency for a positive perturbation $\delta > 0$ while the imaginary part is constant. The three curves are in excellent agreement for small perturbations, showing also the remarkable agreement of the experimental results with the theoretical ones indicating that this is a viable practical solution to make ultra-sensitive sensors. The perturbation δ (the relative change in capacitance C_1) is experimentally introduced through changing the *positive* voltage level of the pump voltage $v_p(t)$. In such a design, each 5 mV change in the positive level of the pump voltage will result in 1% change of the C_1 capacitor value corresponding to $\delta = 0.01$ (see the Supplemental Material). The experimental results (green triangles) in Fig. 5(a) represent the peaks of the fast Fourier transform (FFT) of the measured voltage $v(t)$ of Node A with respect to the ground. The FFT in Fig. 5(b) is taken over the time domain interval corresponding to the “ON” state of the circuit, i.e., during $727 \mu\text{s}$ which correspond to 80% of 1.1 KHz, while $v_{reset} = 0$ V (see Supplemental Material). The results in Fig. 5 demonstrate theoretically and experimentally that for a small perturbation δ , the real part of the resonance frequency is significantly changed and that it can be easily detected even in real noisy electronic systems. Indeed, the spectral width of the measured peaks is small enough to even distinguish the difference between $\delta = 0$ and $\delta = 0.003$. We also increased the repetition frequency and observed the linear-growth saturation of the system under the EPD regime, and by doing the Fourier transform of the time domain signal in the four cases over a time window of length 2 ms (which included the saturation regime); this provided the same results provided in Fig. 5(a) and (b). This latter test showed that the circuit can be operated even includ-

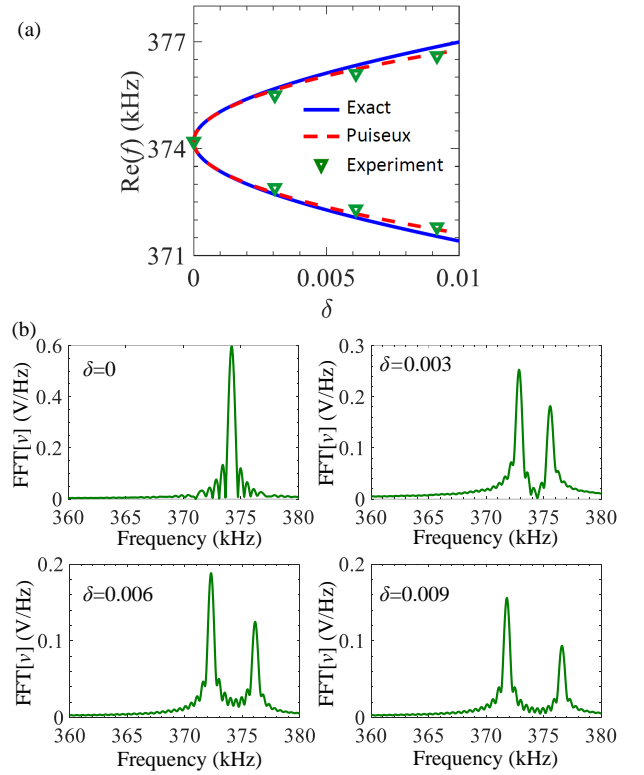


Figure 5. (a) Proof of exceptional sensitivity. Experimental and theoretical changes in the real part of the two resonance frequencies f_p due to a positive relative perturbation δ applied to the capacitance C_1 of the time-varying capacitor (i.e., as $(1 + \delta)C_1$). The two real frequencies *greatly depart* from the EPD frequency around 374 kHz even for very small variation of the capacitance following the fractional power expansion $\Delta f = f_p(\delta) - f_{es} \propto \sqrt{\delta}$. The solid blue line, dashed red line and green symbols represent the calculated-exact, Puiseux series approximation, and experimental resonance frequencies of the LTP LC circuit shown in the Fig. 1(a). The EPD frequency around 374 kHz corresponds to point #1 (blue circle) at the edge of the BZ in Fig. 4(a). (b) Fast Fourier transform of the measured capacitor voltage $v(t)$, obtained at the EPD point and at three different perturbations of the capacitor C_1 . The four spectra correspond to the experimental green triangles in Fig. (a) and they show the resonance frequency shifts due to the capacitor’s perturbation.

ing the saturation regime and it would still provide enhanced sensitivity to perturbation. In conclusion, these experimental results unequivocally demonstrate the exceptional sensitivity of the proposed system operating at an EPD and the practicality of the LTP-resonator circuit to conceive a new class of extremely sensitive sensors.

C. Discussion

A perturbation of the single resonator with an LTP component (for instance a perturbation of the C_1 value of the time-varying capacitance), perturbs the system away from the EPD. In absence of loss, such a per-

turbation results in two real-valued, shifted resonance frequencies $f_p(\delta)$. When losses are present the EPD frequency f_{es} is slightly complex (see Sec. II) and the two frequency shifts $\Delta f = f_p(\delta) - f_{es}$ are approximately real valued. Instead, in a two-coupled resonator system based on PT symmetry operating at an EPD, perturbing one of the capacitors, for instance the one on the lossy (sensing) side, results in two complex resonance frequencies (the value of α_1 in that case would be complex). The reasons of why the two shifted frequencies are complex in a coupled-resonator circuit relies on the fact that the asymmetry in the capacitances (due to the perturbation) disqualifies the system as PT-symmetric and hence the resonance frequencies are no longer real-valued. However, in the sensitive two-coupled PT-symmetric resonator system presented in [2, 19] a (sensing) capacitance perturbation resulted in two real resonance frequencies because in that system PT symmetry was maintained by manually changing the capacitance on the gain side of the circuit (using a varactor) to exactly balance the capacitance perturbation on the sensing (lossy) side of the circuit.

Nevertheless, in many practical applications, a prior knowledge of how much the sensing capacitance is perturbed is not available since the amount of capacitance perturbation depends on the physical (or chemical/biological) quantity to be measured, and the perturbed frequencies would not be real. The reason of this striking difference between the performance of a PT-symmetric coupled resonator circuit and the proposed LTP single resonator circuit rely on the fact that in the PT symmetry case the Puiseux series coefficient α_1 for one varying capacitance is complex whereas in our case the Puiseux series coefficient α_1 for the varying capacitance is either purely real or purely imaginary, depending on the EPD point considered in the dispersion diagram in Fig. 1.

Another important consideration which shows a possible advantage of our proposed sensing scheme is that the capacitance and inductance values of electronic components are not precisely known, i.e., commercially available components have prescribed tolerances (e.g., 1%, 2%, 5%). This uncertainty affects the exact occurrence of the EPD in a PT-symmetric system and in turn it would affect its sensitivity to perturbations. On the contrary, in our case, the tuning of the modulation frequency would generate an EPD regardless of the precise components values. Note that the exact frequency at which the EPD occurs is not important in sensing applications since the sensitivity is associated to the shift from such an EPD frequency, and only the precise measurement if the shift is required.

Finally, it is important to note that electronic and thermal noise in the proposed circuit did not compromise the capability to experimentally verify the high sensitivity of the LTP single-resonator circuit to a system perturbation, as clearly demonstrated in Fig. 5. The resonance peaks in Fig. 5(b) obtained from the measurement of the time domain voltage waveform are very distinguishable

from each other, and their spectral width is much narrower than the frequency shift associated to even 0.3% variation of the perturbed capacitance. Therefore, this paper shows the experimental proof of the existence of EPDs in a single resonator circuit with a LTP modulation of a component, and also the high sensitivity of the system's resonances to perturbations, regardless of the presence of noise. Despite the topic of using EPDs to enhance sensitivity is still subject to some debate, see for instance [40–45], our experimental results clearly show that in some respect it is possible to observe the special sensitivity provided by the square root behavior $\sqrt{\delta}$ when $|\delta| \ll 1$, proper of an EPD, even in presence of realistic noise in the electronic system. Sensitivity to perturbations could be further enhanced by understanding how the parameter α_1 could be increased by an improved design of the system's components.

IV. CONCLUSION

We have shown the first practical and experimental demonstration of exceptional points of degeneracy (EPDs) directly induced via time modulation of a component in a single resonator. This is in contrast to EPDs realized in PT-symmetric systems that would require two coupled resonators instead of one, and the precise knowledge of gain and loss in the system as well as the values of L and C components to have a high quality PT-symmetric resonator. Instead, in our proposed LTP-based scheme we have shown that controlling the modulation frequency of a component in a single resonator is a viable strategy to obtain EPDs since varying a modulation frequency in a precise manner is common practice in electronic systems. The occurrence of a second-order EPD has been shown theoretically and experimentally in two ways: by reconstructing the dispersion diagram of the system resonance frequencies, and by observing the linear growth of the capacitor voltage. We have also experimentally demonstrated how such a temporally induced EPD renders a simple LC resonating system exceptionally sensitive to perturbations of the system capacitance, and how the measurement of the shifted frequencies is robust with respect to the presence of noise. Therefore, the excellent agreement between measured and theoretical sensitivity results demonstrate that the new scheme proposed in this paper is a viable solution for enhancing sensitivity, paving the way to a new class of ultra sensitive sensors that can be applied to a large variety of problems where the occurrence of small quantity of substances shall be detected.

It is important to observe that there are fundamental differences between using the PT symmetry based circuit discussed in [2, 17, 19] and the LTP circuit demonstrated in this paper, in detecting small perturbations of a circuit element: (i) in the PT-symmetric based circuit with two resonators, when the capacitance on one of the resonators is varied the circuit is not PT-symmetric anymore and

the two perturbed resonance frequencies caused by the change of that capacitance are always *complex*-valued; instead in our case, a perturbation of the capacitance leads to two real-valued frequency shifts from the EPD one, and this may have very important implications in sensing technology; (ii) our EPD is easy to obtain by simply modifying the modulation frequency; (iii) the capability to obtain EPDs is not sensitive to tolerances of realistic components since we only need to tune the modulation frequency to obtain an EPD (this is not true in

PT symmetry systems where multiple components needs to have precise values at the same time).

ACKNOWLEDGMENTS

This material is based upon work supported by the National Science Foundation under Award No. ECCS-1711975.

-
- [1] P.-J. Chen, S. Saati, R. Varma, M. S. Humayun, and Y.-C. Tai, *Journal of Microelectromechanical Systems* **19**, 721 (2010).
- [2] P.-Y. Chen, M. Sakhdari, M. Hajizadegan, Q. Cui, M. M.-C. Cheng, R. El-Ganainy, and A. Alu, *Nature Electronics* **1**, 297 (2018).
- [3] T. Q. Trung, S. Ramasundaram, B.-U. Hwang, and N.-E. Lee, *Advanced materials* **28**, 502 (2016).
- [4] Y. Feng, L. Xie, Q. Chen, and L.-R. Zheng, *IEEE Sensors Journal* **15**, 3201 (2015).
- [5] P.-J. Chen, D. C. Rodger, S. Saati, M. S. Humayun, and Y.-C. Tai, *Journal of Microelectromechanical Systems* **17**, 1342 (2008).
- [6] M. Yvanoff and J. Venkataraman, *IEEE Transactions on Antennas and Propagation* **57**, 885 (2009).
- [7] L. Y. Chen, B. C.-K. Tee, A. L. Chortos, G. Schwartz, V. Tse, D. J. Lipomi, H.-S. P. Wong, M. V. McConnell, and Z. Bao, *Nature communications* **5**, 5028 (2014).
- [8] S. Corrie, J. Coffey, J. Islam, K. Markey, and M. Kendall, *Analyst* **140**, 4350 (2015).
- [9] P. Tseng, B. Napier, L. Garbarini, D. L. Kaplan, and F. G. Omenetto, *Advanced Materials* **30**, 1703257 (2018).
- [10] Y. J. Zhang, H. Kwon, M.-A. Miri, E. Kallos, H. Cano-Garcia, M. S. Tong, and A. Alu, *Physical Review Applied* **11**, 044049 (2019).
- [11] H. Kazemi, A. Hajiaghajani, M. Y. Nada, M. Dautta, M. Alshetaiwi, P. Tseng, and F. Capolino, arXiv:1909.03344 (2019).
- [12] M. A. K. Othman, F. Yazdi, A. Figotin, and F. Capolino, *Phys. Rev. B* **93**, 024301 (2016).
- [13] M. Y. Nada and F. Capolino, *J. Opt. Soc. Am. B* **37**, 2319 (2020).
- [14] M. Veysi, M. A. K. Othman, A. Figotin, and F. Capolino, *Physical Review B* **97**, 195107 (2018).
- [15] H. Hodaei, M.-A. Miri, M. Heinrich, D. N. Christodoulides, and M. Khajavikhan, *Science* **346**, 975 (2014).
- [16] D. Oshmarin, F. Yazdi, M. A. Othman, J. Sloan, M. Radfar, M. M. Green, and F. Capolino, *IET Circuits, Devices & Systems* (2019).
- [17] J. Schindler, A. Li, M. C. Zheng, F. M. Ellis, and T. Kottos, *Physical Review A* **84**, 040101 (2011).
- [18] M. Chitsazi, H. Li, F. Ellis, and T. Kottos, *Physical Review Letters* **119**, 093901 (2017).
- [19] M. Sakhdari, M. Hajizadegan, Y. Li, M. Cheng, J. C. H. Hung, and P.-Y. Chen, *IEEE Sensors Journal* **18**, 9548 (2018).
- [20] M. Sakhdari, M. Hajizadegan, Q. Zhong, D. Christodoulides, R. El-Ganainy, and P.-Y. Chen, *Physical Review Letters* **123** (2019), 10.1103/physrevlett.123.193901.
- [21] J. Wiersig, *Physical Review Letters* **112**, 203901 (2014).
- [22] J. Wiersig, *Physical Review A* **93**, 033809 (2016).
- [23] H. Hodaei, A. U. Hassan, S. Wittek, H. Garcia-Gracia, R. El-Ganainy, D. N. Christodoulides, and M. Khajavikhan, *Nature* **548**, 187 (2017).
- [24] W. Chen, S. Kaya Ozdemir, G. Zhao, J. Wiersig, and L. Yang, *Nature* **548**, 192 (2017).
- [25] C. M. Bender and S. Boettcher, *Physical Review Letters* **80**, 5243 (1998).
- [26] T. Stehmann, W. D. Heiss, and F. G. Scholtz, *Journal of Physics A: Mathematical and General* **37**, 7813 (2004).
- [27] M. Y. Nada, H. Kazemi, A. F. Abdelshafy, F. Yazdi, D. Oshmarin, T. Mealy, A. Figotin, and F. Capolino, in *2018 18th Mediterranean Microwave Symposium (MMS) (IEEE, 2018)* pp. 108–111.
- [28] M. Y. Nada, M. A. K. Othman, and F. Capolino, *Physical Review B* **96**, 184304 (2017).
- [29] M. A. K. Othman, M. Veysi, A. Figotin, and F. Capolino, *Physics of Plasmas* **23**, 033112 (2016).
- [30] A. Figotin and I. Vitebskiy, *Physical Review E* **72** (2005), 10.1103/physreve.72.036619.
- [31] M. Y. Nada, A. F. Abdelshafy, T. Mealy, F. Yazdi, H. Kazemi, A. Figotin, and F. Capolino, in *2018 International Conference on Electromagnetics in Advanced Applications (ICEAA) (IEEE, 2018)* pp. 627–629.
- [32] H. Kazemi, M. Y. Nada, T. Mealy, A. F. Abdelshafy, and F. Capolino, *Phys. Rev. Applied* **11**, 014007 (2019).
- [33] A. Welters, *SIAM Journal on Matrix Analysis and Applications* **32**, 1 (2011).
- [34] J. A. Richards, *Analysis of periodically time-varying systems* (Springer, New York, 1983).
- [35] A. Ashkin, J. S. Cook, W. H. Louisell, and C. F. Quate, “Parametric amplifier,” (1960), US Patent 2,958,001.
- [36] E. Cassedy and A. Oliner, *Proceedings of the IEEE* **51**, 1342 (1963).
- [37] E. M. T. J. R. C. Honey, *IEEE Transactions on Microwave Theory and Techniques* **8**, 351 (1960).
- [38] J.-C. Lee, H. Taylor, and K. Chang, *IEEE Microwave and Guided Wave Letters* **7**, 267 (1997).
- [39] T. Yamamoto, K. Inomata, M. Watanabe, K. Matsuba, T. Miyazaki, W. D. Oliver, Y. Nakamura, and J. S. Tsai, *Applied Physics Letters* **93**, 042510 (2008).
- [40] W. Langbein, *Physical Review A* **98**, 023805 (2018).
- [41] M. Zhang, W. Sweeney, C. W. Hsu, L. Yang, A. Stone, and L. Jiang, *Physical Review Letters* **123**, 180501

- (2019).
- [42] H.-K. Lau and A. A. Clerk, *Nature Communications* **9**, 4320 (2018).
- [43] J. Wiersig, *Nature Communications* **11**, 2454 (2020).
- [44] J. Wiersig, *Physical Review A* **101**, 053846 (2020).
- [45] Z. Xiao, H. Li, T. Kottos, and A. Alù, *Physical Review Letters* **123**, 213901 (2019).

Experimental Demonstration of Exceptional Points of Degeneracy in Linear Time Periodic Systems and Exceptional Sensitivity

Hamidreza Kazemi, Mohamed Y. Nada, Alireza Nikzamir, Franco Maddaleno, and Filippo Capolino

We first define the time-varying capacitance based on the multiplier concept in Fig. 3(a) in the main text and show that its definition leads to an LC circuit described by differential equations consistent to the previous theory shown in [1], hence leading to the occurrence of exceptional points of degeneracy (EPDs). Then we discuss the physical implementation of the electronic linear time periodic (LTP) LC resonator with a time varying capacitor and reset signal.

The LTP LC resonator circuit shown in Fig. 3(c) in the main text is composed of two subsystems: i) the sensing device which comprises of a time variant LC resonator operating at the time-induced EPD [1], and ii) a reset mechanism to stop the growing oscillation amplitude and to set the initial voltage of the capacitor at the beginning of each operation regime to avoid saturating the circuit. The schematic and detailed working principle of each subsystem is explained in the following sections.

I. TIME VARYING CAPACITANCE AND FUNDAMENTAL DYNAMIC EQUATIONS

The time varying capacitance is obtained by resorting to the multiplier scheme in Fig. 3(a) in the main text. Without worrying for a moment about the physical implementation and the reset scheme that are explained in the following sections, we shall observe here that the voltage $W(t)$ is given by the product $W(t) = v(t)v_p(t)/V_0$, where the term V_0 is a constant coefficient of the multiplier that is used to normalize its output voltage. Since in this paper the signal $v_p(t)$ is a square wave with frequency f_m , it experiences jumps (discontinuities), implying that also $W(t)$ is discontinuous. The voltage applied to the capacitor C_0 is then given by $v_c(t) = v(t) - W(t) = v(t)(1 - v_p(t)/V_0)$. This capacitor voltage cannot be discontinuous in time, hence $v_c(t)$ is a continuous function and indeed $v(t)$ carries the same discontinuities as $W(t)$.

We define the capacitance of the synthesized time varying capacitor used in this paper as $C(t) = q(t)/v(t)$, where $q(t)$ is the charge on the capacitor. The same charge is also given by $q(t) = C_0v_c(t)$, leading to the value of the time varying capacitance $C(t) = C_0v_c(t)/v(t)$. Substituting for $v_c(t)$ in this latter equation leads to $C(t) = C_0(1 - v_p(t)/V_0)$ that is the synthesized piece wise time varying capacitance with period T_m .

The two fundamental differential equations describing the LTP LC circuit in Fig. 3(a) in the main text are $dq/dt = i_c(t) = -i(t)$ and $di/dt = v(t)/L_0 = q(t)/(L_0C(t))$, that in matrix form are rewritten as

$$\frac{d}{dt} \begin{pmatrix} q \\ i \end{pmatrix} = \begin{pmatrix} 0 & -1 \\ \frac{1}{L_0C(t)} & 0 \end{pmatrix} \begin{pmatrix} q \\ i \end{pmatrix}. \quad (1)$$

This first order differential equation is the same as that considered in Eq. (1) in the main text and in [1] and therefore it leads to the same dynamic current and voltage of the LTP LC circuit studied in [1], including the occurrence of EPDs.

II. DESIGN AND IMPLEMENTATION OF THE TIME-VARYING CAPACITANCE

The scheme of the proposed sensor (i.e., the time varying LC resonator) is based on the design of a synthesized periodic time-varying capacitance $C(t)$ that switches between two values C_1 and C_2 with a modulation frequency f_m where the parameters C_1 , C_2 and f_m need to be tunable. In order to make such a time-varying capacitor, we use a regular time-invariant capacitor C_0 which is connected in parallel with a multiplier U_1 (AD835 [2]) as shown in Fig. 1(a). In general terms, the multiplier U_1 provides the time domain function

$$W(t) = \frac{(X_1 - X_2)(Y_1 - Y_2)}{V_0} + Z, \quad (2)$$

that is connected to the lower terminal of the capacitor C_0 . Here W , X_1 , X_2 , Y_1 , Y_2 , and Z represent the voltages at the pins denoted with the same symbols of the multiplier U_1 and $V_0 = 1.05$ V is the voltage normalization factor dictated by the multiplier and given in the data sheet [2]. In this circuit schematic, the X_2 and Y_2 pins are both connected to the ground, the pump voltage $v_p(t)$ is applied to the Y_1 pin and the X_1 pin is connected to Node A as shown in Fig. 1(a). Hence, the output function of the multiplier is simplified as

$$W(t) = \frac{X_1v_p(t)}{V_0} + Z. \quad (3)$$

From the schematic and since the X_1 pin input current is zero (it has high input impedance), we express the current flowing into the capacitor C_0 as

$$i_c(t) = C_0 \frac{d}{dt} (X_1 - W). \quad (4)$$

The printed circuit board (PCB) layout and the actual assembled circuit with resonator (capacitor C_0 , inductor L_0 , multiplier chip U_1), chip with switches U_2 , pump voltage $v_p(t)$ and reset $v_{reset}(t)$ connectors, and PCB traces are shown in Fig. 1(b) and (c). In the following we describe the two operation regimes of the circuit and the principle of the reset mechanism in detail.

III. REGIMES OF OPERATION

The proposed circuit has two distinct phases (regimes) of operation which are differentiated based on the status of the reset signal v_{reset} . Reset signal v_{reset} is a digital clock coming from an external waveform generator that is used to stop the oscillation of the time-varying LC resonator when it is high level voltage (logic Level 1), and allows the resonator circuit to run when it is at low level voltage (logic Level 0). These two different operation regimes are described in the following.

(i) *LTP-LC operating regime with EPD*: During this regime, the reset signal is a logic low (logic Level 0) so that the time varying LC resonator is allowed to have a free run, i.e., its voltage is varying as in a time varying LC resonator with a given initial voltage condition. During this regime, low level voltage v_{reset} causes Switch 1 to be “on”, hence the pin Z of the multiplier U_1 shown in Fig. 1(a), is connected to the ground (see section IV) while Switch 4 is off, therefore, the input $X_1 = v(t)$. In this case, by using Eq. (3), the multiplier output is $W(t) = v(t)v_p(t)/V_0$. Therefore the voltage difference at the two ends of the capacitor C_0 is $v_c(t) = v(t) - v(t)v_p(t)/V_0$ and the current flowing into the capacitor is

$$i_c(t) = C_0 \frac{d}{dt} (v(t) - v(t)v_p(t)/V_0), \quad (5)$$

which can be also interpreted as flowing into a synthesized time varying capacitor with applied voltage $v(t)$. Considering a two level piece-wise constant pump voltage $v_p(t)$, where $dv_p(t)/dt = 0$ for $0 < t < 0.5T_m$ and $0.5T_m < t < T_m$, the current flowing into the capacitance is given by

$$i_c(t) = C(t) \frac{dv}{dt} = C_0 (1 - v_p(t)/V_0) \frac{dv}{dt}. \quad (6)$$

It is clear from Eq. (6), that the capacitance seen from Node A towards the ground is time-variant and its shape is dictated by the pump voltage. Considering the pump voltage as

$$v_p(t) = \begin{cases} 0.525 \text{ V} & 0 < t < 0.5T_m \\ -0.525 \text{ V} & 0.5T_m < t < T_m \end{cases}, \quad (7)$$

and recalling that $V_0 = 1.05 \text{ V}$, the time varying capacitance from Eq. (6) is

$$C(t) = \begin{cases} 0.5C_0 & 0 < t < 0.5T_m \\ 1.5C_0 & 0.5T_m < t < T_m \end{cases}. \quad (8)$$

We observe from Eqs. (6)-(8), that a change of 5 mV in the high level of the pump voltage $v_p(t)$ will result in approximately a relative change of 1% in the capacitance value C_1 , i.e.,

$$\delta \triangleq \frac{C_{1,perturbed} - C_1}{C_1} \quad (9)$$

$$= \frac{(1 - 0.520/1.05)C_0 - 0.5C_0}{0.5C_0} \approx 1\% \quad (10)$$

(ii) *Reset regime*: During this regime, the reset signal is a logic high (logic Level 1), therefore Switch 4 is “on” and S_4 takes the value of D_4 that is grounded. As a result Node A is connected to the ground and the operation of the time-varying LC resonator is halted. Moreover, during this regime, the capacitor C_0 is charged again with an initial voltage to be ready for the next *LTP-LC operating regime*. The operation of the reset mechanism circuit is explained in the following section.

IV. RESET AND LTP-LC OPERATING REGIME MECHANISMS

The reset mechanism in this circuit is employed to (i) prevent the saturation of the system due to the growth of the capacitor voltage with time and to (ii) set an initial voltage on the capacitor C_0 in order to start a new *LTP-LC operating regime*. The reset mechanism is implemented using the ADG4613 chip which contains four independent single pole/single throw (SPST) switches [5], denoted by U_2 in the Supplementary Fig. 1(a). This figure shows the four switches where IN, D, and S represent the control input, input, and output of the switches, respectively. Two switches (1 and 3) are turned on with logic Level 1 (high level voltage of v_{reset}) on the appropriate control input, implying that during that time S_1 and S_3 take the value of terminals $D_1 = 0 \text{ V}$ and D_3 , respectively, and they are open when they are “off”. Switch 3 is not used in our physical implementation. The logic is inverted on the other two switches (2 and 4), i.e., the switches turn on with logic Level 0 (low level voltage of v_{reset}) on their control input implying that during that time S_2 and S_4 take the value imposed at terminals $D_2 = V_+R_1/(R_1 + R_2)$, and $D_4 = 0 \text{ V}$, respectively. In the reset mechanism we use only Switches 1, 2, and 4 where the control input of these switches is connected to a digital clock signal v_{reset} as indicated in Supplementary Fig. 1(a). The reset signal is a digital clock with 20% duty cycle, i.e., $v_{reset} = 2 \text{ V}$ for 20% of its period (logic Level 1) and $v_{reset} = 0 \text{ V}$ otherwise (logic Level 0). Therefore, the LTP LC resonator is showing an oscillating output for 80% of the reset signal period. In

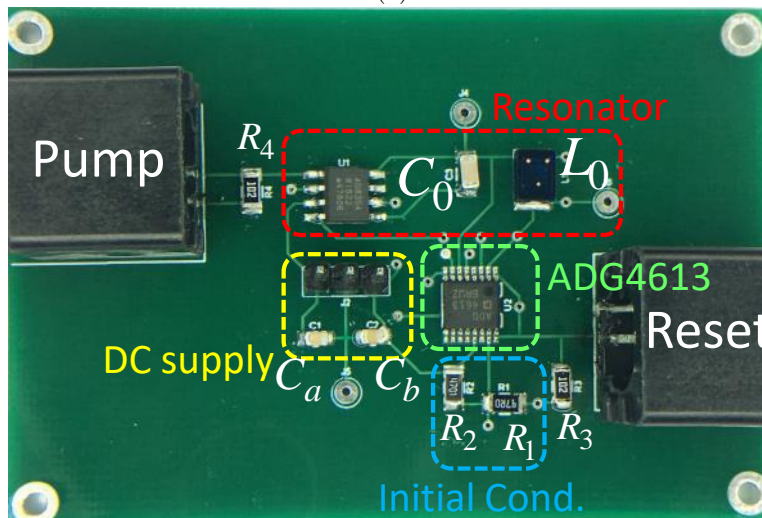
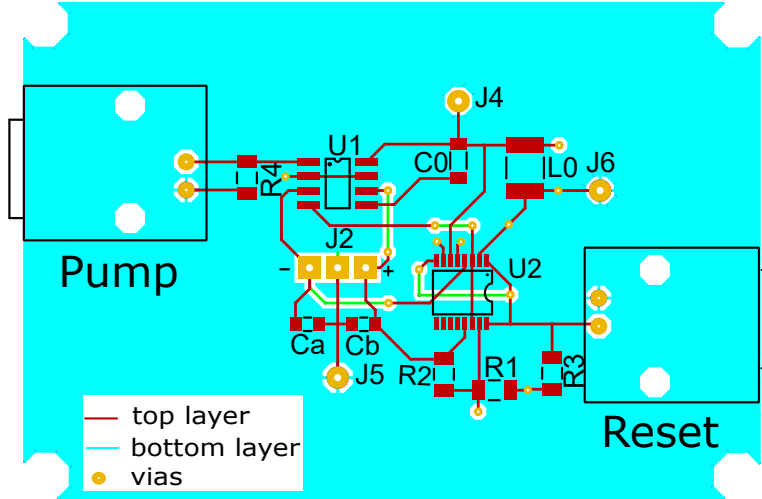
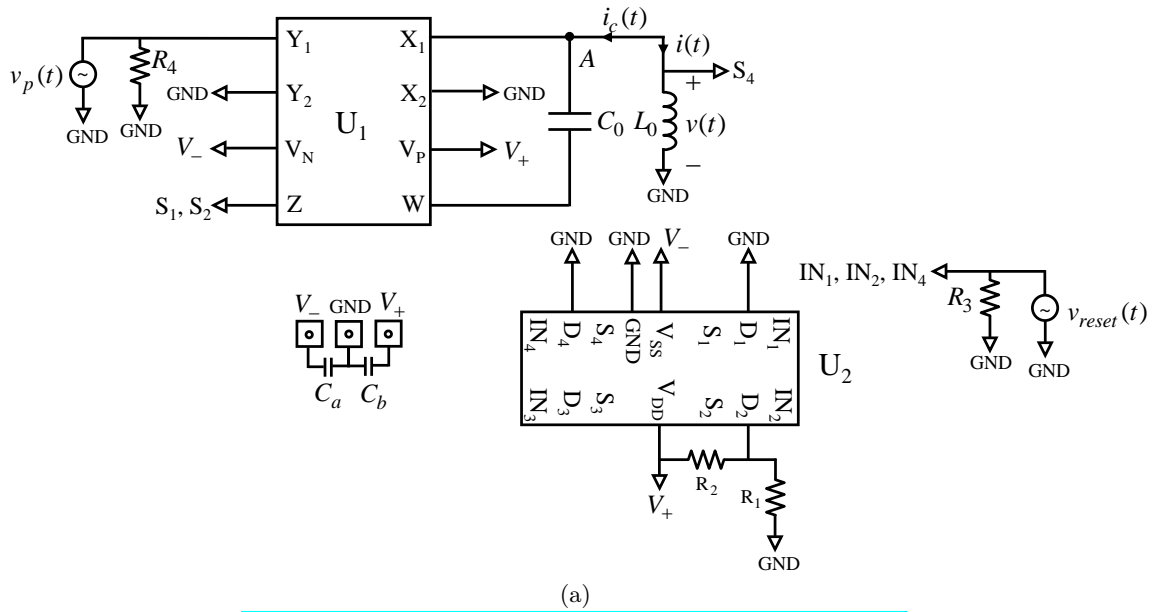


Figure 1. (a) Schematic of the time-varying LC resonator circuit based on the capacitor $C_0 = 10$ nF (NP0 1206 [3]), the inductor $L_0 = 33$ μ H (MSS7348-333ME [4]), the multiplier U_1 and the reset mechanism circuit U_2 . (b) PCB layout of the assembled circuit where the top layer traces are in red, the ground plane is in cyan, the bottom traces are in green, and the connecting vias are in orange. In this design Via J_4 is a probe point for the capacitor voltage, whereas Vias J_5 and J_6 are test points connected to the ground plane and are used to connect the ground of the measurement equipment to the ground of the circuit. All the ground nodes are connected to each other using the bottom cyan layer. (c) Fabricated PCB and assembled circuit with blocks highlighted.

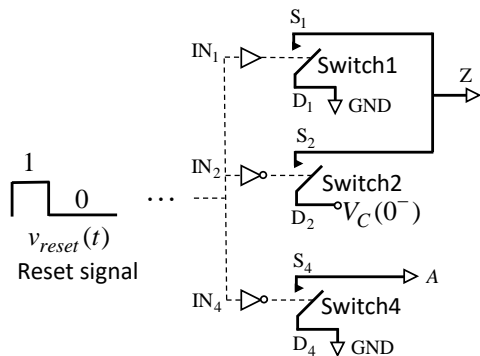


Figure 2. The three switches used for establishing the two regimes of operation: the LTP LC resonator regime with EPD and the reset mechanism that at the same time is also charging the capacitor C_0 with an initial voltage to be used to start the next LTP LC resonator regime. These switches are Switch 1, 2, and 4 of U_2 shown in Fig. 1 and their control inputs IN_1 , IN_2 , and IN_4 are connected to the reset signal $v_{reset}(t)$. The outputs of Switch 1 and 2, S_1 and S_2 , are both connected to the pin Z of the U_1 , and S_2 is used to provide the initial voltage of the capacitor at the beginning of each operating LTP LC regime. The output S_4 of Switch 4 is connected to Node A and is used to set the short the inductor when the reset signal $v_{reset}(t)$ is at high voltage (logic Level 1).

summary, during the 80% of the $v_{reset}(t)$ period the circuit has $S_1 = 0\text{ V}$, while the S_2 and S_4 are open circuits, implying that $Z = 0\text{ V}$ and $X_1 = v(t)$, whereas during the remaining 20% of the reset signal period, the circuit has $S_2 = V_+R_1/(R_1 + R_2)$ and $S_4 = 0\text{ V}$ while S_1 is left open, implying that $Z = S_2$ and $X_1 = 0\text{ V}$.

A. Halting the oscillation

As described, one of the benefits of the reset mechanism circuit is to stop the time-varying LC resonator

operating at an EPD before it reaches saturation. For this purpose, during the *reset regime*, Switch 4 is used to short Node A to the ground when the reset signal v_{reset} is at logic Level 1. Indeed the reset signal logic Level 1 is connected to the input control IN_4 which turns on Switch 4 connecting S_4 to the ground. Since Node A is connected to S_4 , the voltage across the inductor L_0 is set to zero preventing the oscillation.

B. Setting the initial voltage condition on the capacitor C_0

During each *reset regime* just described, Node A is grounded therefore the voltage oscillation is halted, and the inductor current decays with a short transient. In order to start a new *LTP LC operating regime* after each *reset regime*, it is necessary to provide the capacitor with the initial voltage. This is done by using Switch 2 of the ADG4613 shown in the Supplementary Figure 2 with its control input IN_2 connected to v_{reset} . Since S_2 is connected to the Z pin, during this *reset regime* time we have $Z = V_+R_1/(R_1 + R_2)$, and Z represents the summing input of the voltage multiplier as shown in Eq. (2). Furthermore since Node A is grounded, we have $X_1 = 0\text{ V}$, resulting in $W = Z = V_+R_1/(R_1 + R_2)$, i.e., the capacitor is inversely charged. An initial capacitor voltage $V_C(0^-) = -V_+R_1/(R_1 + R_2) = -50\text{ mV}$ is produced by the voltage divider using $R_1 = 47\ \Omega$ and $R_2 = 4.7\text{ k}\Omega$ and by the positive DC supply $V_+ = 5\text{ V}$ shown in the Supplementary Fig. 1(a).

[1] H. Kazemi, M. Y. Nada, T. Mealy, A. F. Abdelshafy, and F. Capolino, Phys. Rev. Applied **11**, 014007 (2019).
 [2] *250 MHz, Voltage Output, 4-Quadrant Multiplier*, Analog Devices (2019), rev. E.
 [3] *Surface Mount Ceramic Capacitor Products*, AVX Corporation (2019).

[4] *Shielded Power Inductors-MSS7348*, Coilcraft Inc. (2018).
 [5] *Power-Off Protection $\pm 5\text{ V}$, $+12\text{ V}$, Quad SPST Switches with 5 Ohms On Resistance*, Analog Devices (2019), rev. 0.